JOURNAL OF GEOPHYSICAL RESEARCH, VOL. 111, C11S05, doi:10.1029/2005JC003253, 2006

A numerical study on dynamic mechanisms of seasonal temperature variability in the Yellow Sea

Dejun Dai,[1,2] Fangli Qiao,[1,2] Changshui Xia,[1,2] and Kyung Tae Jung[3]

Received 28 August 2005; revised 13 July 2006; accepted 9 August 2006; published 31 October 2006.

[1] Using in situ observations and numerical modeling, this study investigates the dynamical mechanisms of seasonal variability of water temperature in the Yellow Sea (YS). Observations indicate that bottom temperature lags 3–4 months behind surface temperature in reaching a maximum in the central YS. Wave-tide-circulation coupled model simulates this time lag and indicates that the diffusion process is a key factor governing the temperature variation below the surface layer. Based on the diffusion equation of temperature, a scheme is developed to estimate the vertical diffusion coefficient. At an observation station located at 36°00′N 124°00′E, the diffusion coefficients from April to September are estimated by using the temperature data from 1954 to 1985. The mean diffusion coefficient (MDC) in the upper layer from 0 m to 15 m is almost one order of magnitude larger than those in the middle layer from 20 to 40 m, except in April. In the middle layer, the MDC is inversely proportional to the squared buoyancy frequency, and the mean value of MDC averaged from June to September is 0.28 $cm^2\ s^{-1}$. The inverse proportionality agrees with the Osborn's relation, which has been used to estimate the diapycnal diffusivity.

Citation: Dai, D., F. Qiao, C. Xia, and K. T. Jung (2006), A numerical study on dynamic mechanisms of seasonal temperature variability in the Yellow Sea, *J. Geophys. Res.*, *111*, C11S05, doi:10.1029/2005JC003253.

1. Introduction and Background

[2] The Yellow Sea (YS) is a semi-enclosed basin, with a horizontal scale of about 400 km by 800 km and a maximum depth of about 85 m as shown in Figure 1. The thermal structure in the YS has drawn a lot of interest because of its significance in the physical oceanography, the biological environment, and acoustic properties. *He et al.* [1959] and *Miao et al.* [1991] studied the generation mechanism of Yellow Sea Cold Water Mass (YSCWM). *Kwan* [1963], *Yuan* [1979], *Yuan and Li* [1993], *Feng et al.* [1992], and *Su and Huang* [1995] discussed the thermal structure and circulation pattern in the YSCWM. Numerical methods were also developed to simulate and predict the vertical thermal structure in the YSCWM using a similarity function of the vertical temperature profile [*Wang et al.*, 1996a, 1996b; *Jin et al.*, 1996].

[3] Since the YS is a broad and shallow basin, the entire water column in it is directly exposed to seasonal atmospheric forcing. In fact, water temperature from the top to the bottom shows an obvious seasonal variability. *Chu et al.* [1997] developed a thermal parametric model based on a layered temperature fields (including a mixed layer, thermocline, and deep layers) to study the characteristics of such seasonal temperature variation. Their further study found that surface heat flux accounts for the water temperature variation [*Chu et al.*, 2005]. However, the question, how does the ocean dynamically respond to atmospheric forcing, still remains unclear.

[4] We have collected temperature observations in the YS and Bohai Sea from 1954 to 1985. Figure 2 shows annual temperature variations at Station A (36°00′N 124°00′E) (location shown in Figure 1). One can see that the surface temperature reached a maximum of 26.0°C in mid-August. After a time lag of 4 months, the bottom temperature reached its maximum of 9.5°C in mid-December. This regular phase lag in temperature was also observed at different stations in the YS by previous investigators [*Kwan*, 1963]. The maximum bottom temperature had phase propagation (Figure 3). In the coastal region, the maximum of bottom temperature occurred in September while in the central region, the maximum occurred in November or December. The time delay is a universal phenomenon in the YS rather than a peculiar case occurring only from 1954 to 1985 [*Su and Yuan*, 2005]. The surface temperatures always reach their maximums in mid-August, this implies that the maximums at the bottom lags 3–4 months behind those at the surface in the central YS. So far, however, the dynamic mechanism of this phenomenon has not yet been explored. Therefore, this study aims to gain an insight into the dynamics that controls the temperature variation below the surface layer using numerical modeling methods.

[5] The simulated results from wave-tide-circulation coupled model are given in the next section. Section 3 gives the

[1]The First Institute of Oceanography, State Oceanic Administration (SOA), Qingdao, China.

[2]Key Laboratory of Marine Science and Numerical Modeling (MASNUM), SOA, Qingdao, China.

[3]Korea Ocean Research and Development Institute, Ansan, Korea.

0148-0227/06/2005JC003253$09.00

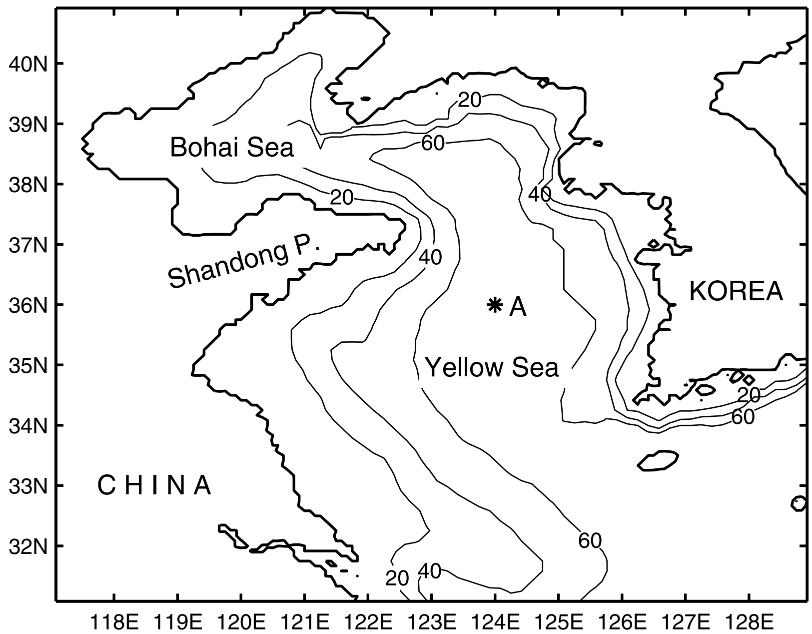

Figure 1. Topography of the Yellow Sea and Bohai Sea (the contour interval is 20 m). The asterisk shows the location of Station A, where the water depth is 79 m.

diffusion coefficients estimated from the observed temperatures at Station A using a scheme based on temperature diffusion equation. Results are discussed and summarized in sections 4 and 5.

2. Results From the MASNUM Coupled Model

[6] The wave-tide-circulation coupled model used in this study, was developed in the Key Laboratory of Marine Science and Numerical Modeling (MASNUM) [*Qiao et al.*, 2004a, 2004b; *Xia et al.*, 2006]. The circulation part of the model is adapted from the Princeton Ocean Model (POM), which embeds a 2.5-level turbulence closure scheme to calculate the vertical turbulence mixing [*Mellor and Yamada*, 1982]. As a common problem, the turbulence closure scheme underestimates surface mixing, so that the simulated mixed layer depth is unrealistically shallow. Thus the sea surface temperature is overestimated, especially in summer [*Martin*, 1985; *Kantha and Clayson*, 1994; *Ezer*, 2000; *Mellor*, 2001]. *Qiao et al.* [2004a, 2004b] suggested that wave-induced mixing plays a key role in formation of the upper mixed layer, especially in spring and summer, and introduced it into the numerical simulation. In order to improve the upper mixed layer simulation, the coupled model embeds a MASNUM wave-number spectral scheme (once called LAGFD-WAM) [*Yuan et al.*, 1991], which is used to calculate a wave-induced mixing parameter Bv. Then, Bv is added to the vertical viscosity K_M and diffusivity K_H, which are calculated by the 2.5-level turbulence closure model in POM. In addition, tidal currents are considered to be important in inducing strong bottom mixing in a shallow water region. Thus, a tidal current simulation is also included in the model.

[7] To reduce the influence of open boundary conditions, the computational domain covers the Bohai Sea, YS, East China Sea (ESC), South China Sea (SCS) and a portion of the northwest Pacific. The horizontal resolution is 1/6° × 1/6°. With a fine resolution in the upper layers, the 16 vertical sigma layers from the surface to the bottom are 0.000, −0.003, −0.006, −0.013, −0.025, −0.050, −0.100, −0.200, −0.300, −0.400, −0.500, −0.600, −0.700, −0.800, −0.900, and −1.00. The model is forced by monthly climatological wind stress, net heat flux, and evaporation minus precipitation (E-P) from the Comprehensive Ocean-Atmosphere Data Set (COADS) [*da Silva et al.*, 1994a, 1994b].

[8] Open lateral boundary conditions (temperature, salinity, sea level, and velocity), initial sea level, and current

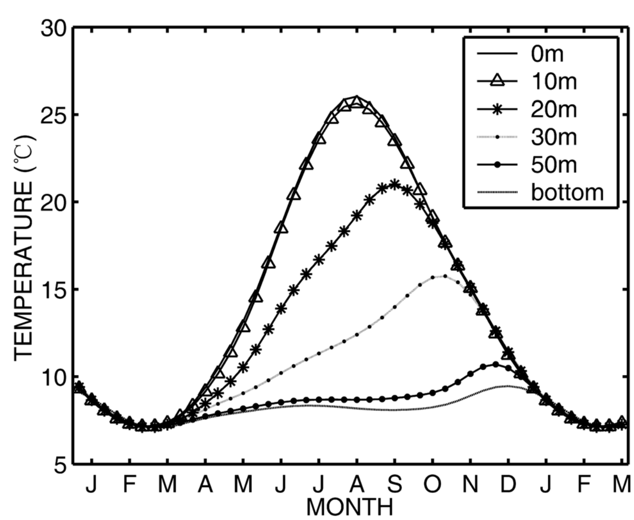

Figure 2. Seasonal variations of water temperature in different levels at Station A.

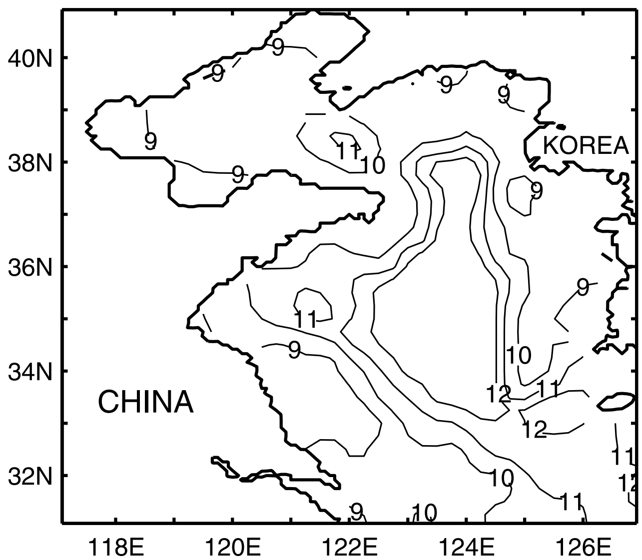

Figure 3. The month in which the observed bottom temperature reaches its maximum. Numerals on the isolines represent months: 9, September; 10, October; 11, November; 12, December.

fields are provided by a global 1/2° × 1/2° MASNUM model output after interpolating them onto the model grids [*Xia et al.*, 2004a, 2004b]. The annual mean Levitus climatology [*Levitus*, 1982] is used for initial temperature and salinity conditions. The Yangtze River runoff is included as a boundary condition [*Qiao et al.*, 2004a], which comes from a monthly climatological data set constructed from a 35-year river discharge record at the Datong Observation Station. The model spins up for 6 years and the results of the last year are used to study the seasonal variability of temperature. The tidal currents, circulation, salinity, and temperature of YSCWM have been analyzed and validated by the observations [*Qiao et al.*, 2004a; *Xia et al.*, 2006].

[9] The model simulates spatial patterns and temporal variability of temperature well. An evident improvement is that the modeled upper mixed layer is much more reasonable than the result generated by the original POM model [*Qiao et al.*, 2004a, 2004b]. Figure 4 shows the simulation results for month in which the bottom temperature reaches its maximum (peak month). The peak month changes gradually from September near the coastal water to December in the central YS. One can see that the general patterns displayed in Figure 4 are similar to those of Figure 3, with only minor differences in fine details. Moreover, the isolines of the peak month in Figures 3 and 4 are almost parallel to the isobaths (Figure 1), implying that diffusion might be a key factor controlling the temperature variations below the surface layer. In shallow water, atmospheric heat flux can quickly be transported from the surface to the bottom through diffusion, so that the bottom temperature lags only 1 or 2 months behind the surface temperature in reaching a maximum. In deep water, the thermocline impedes heat flux entering the deep layer, and thus longer time is needed to convey the surface heat flux to the bottom. This point will be analyzed in the following sections.

[10] In Cartesian coordinates, the temperature variation is governed by the following equation

$$\frac{\partial T}{\partial t} + U\frac{\partial T}{\partial x} + V\frac{\partial T}{\partial y} + W\frac{\partial T}{\partial z} = \frac{\partial}{\partial z}\left(k_z\frac{\partial T}{\partial z}\right) + \frac{\partial}{\partial x}\left(k_H\frac{\partial T}{\partial x}\right) + \frac{\partial}{\partial y}\left(k_H\frac{\partial T}{\partial y}\right), \tag{1}$$

where x,y,z denote the Cartesian coordinates, T the temperature, U,V,W the velocity components in x,y,z directions respectively, k_z the vertical diffusion coefficient, and k_H the horizontal diffusion coefficient. Scale analysis indicates that the terms $W\frac{\partial T}{\partial z}$, $\frac{\partial}{\partial x}(k_H\frac{\partial T}{\partial x})$ and $\frac{\partial}{\partial y}(k_H\frac{\partial T}{\partial y})$ are much smaller than the terms $U\frac{\partial T}{\partial x}$, $V\frac{\partial T}{\partial y}$ and $\frac{\partial}{\partial z}(k_z\frac{\partial T}{\partial z})$. Therefore, equation (1) can be reduced to

$$\frac{\partial T}{\partial t} + U\frac{\partial T}{\partial x} + V\frac{\partial T}{\partial y} = \frac{\partial}{\partial z}\left(k_z\frac{\partial T}{\partial z}\right). \tag{2}$$

In order to determine a key factor responsible for the temperature variation, the advection terms or the vertical diffusion term, the ratio of the diffusion term to the sum of advection terms is calculated,

$$r = \frac{\left|\frac{\partial}{\partial z}\left(k_z\frac{\partial T}{\partial z}\right)\right|}{\left|U\frac{\partial T}{\partial x}\right| + \left|V\frac{\partial T}{\partial y}\right|}. \tag{3}$$

In the months when convection occurs, the diffusion coefficient k_z becomes very large, so that the calculation errors about the diffusion term may become large. To reduce the errors, we average the ratios of the diffusion to the advection terms from April to October. The results are

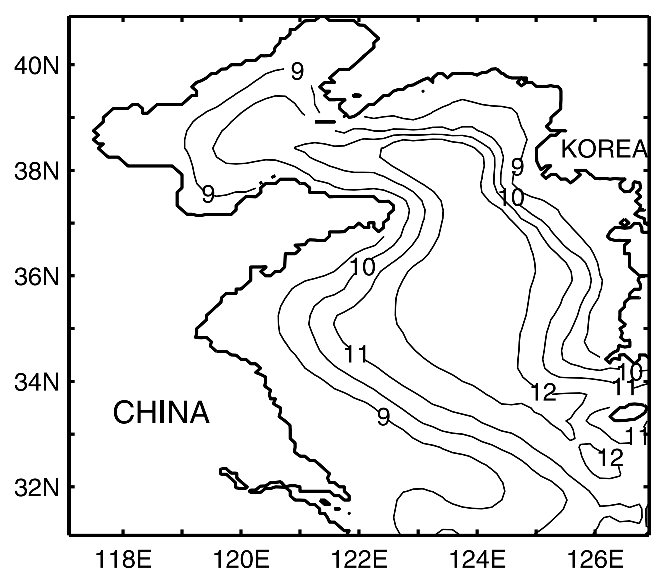

Figure 4. The simulation results for month in which the bottom temperature reaches its maximum. Numerals on the isolines represent months: 9, September; 10, October; 11, November; 12, December.

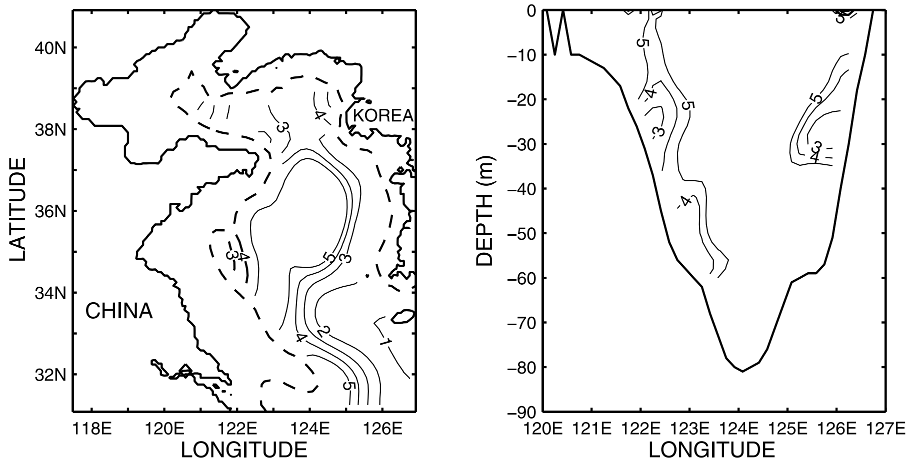

Figure 5. The mean ratio of the diffusion term to the advection terms averaged from April to October at 30 m (left) and along the 36°N transect (right). The dashed line in the left panel represents the 30 m isobath.

shown in Figure 5. The left panel shows the horizontal distribution at the 30 m level. One can see that the mean ratios are larger than 3 in most of the regions, and even larger than 5 in the central YS. Similar results can also be found in the right panel, which shows a vertical transect along 36°N. The large ratios indicate that the diffusion term rather than the advection terms is the dominant factor controlling temperature variation. Hence, equation (2) can be reduced further to

$$\frac{\partial T}{\partial t} = \frac{\partial}{\partial z}\left(k_z \frac{\partial T}{\partial z}\right). \tag{4}$$

[11] The physical processes defined in the Cartesian coordinate are used to identify the dominant factor controlling the temperature variation. However, it is really along-isopycnal advection and diffusion that should be compared with the effects of diapycnal diffusion, rather than strictly horizontal advection and diffusion. Heating by the horizontal advection and diffusion could be much larger in a model than it is in the real ocean because of sloping isopycnal surfaces. In the isopycnal-diapycnal coordinates, it might be even more reasonable to neglect the isopycnal processes.

[12] Observations and numerical results from the coupled model indicate that the isothermal surfaces are almost horizontal in the central YS from April to September [*Qiao et al.*, 2004a; *Su and Yuan*, 2005; *Xia et al.*, 2006], implying that the physical processes defined in the Cartesian coordinates, such as the advection and the diffusion, are equivalent to those defined in the isopycnal-diapycnal coordinates in the central YS. It is therefore reasonable to conclude that the horizontal advection plays a small role compared to the vertical diffusion in the seasonal temperature variation, as shown in Figure 5. The vertical diffusion in equation (4) can be considered as the diapycnal diffusion, k_z, the diapycnal diffusion coefficient in the central YS. However, the contribution of horizontal advections and diffusion to the temperature variation may be much larger in the coastal water because of the sloping isothermal surfaces, i.e., the simplified governing equation (4) for the temperature variation is satisfied only in the central YS.

3. Estimated Diffusion Coefficient at Station A

[13] The above analyses indicate that the diffusion is the dominant process responsible for water temperature variations below the surface layer in the central YS. In order to understand the corresponding dynamical processes, a scheme is established to estimate the diffusion coefficient from temperature observations (see Appendix A). In the scheme, equation (4) is the governing equation for the temperature variation. The surface temperature is specified as the surface boundary condition,

$$T|_{z=0} = T_{surf}(t), \tag{5}$$

and a zero-flux condition at the bottom boundary is specified, i.e.,

$$\frac{\partial T}{\partial z}|_{z=-H} = 0. \tag{6}$$

The cost function for estimating the diffusion coefficient is a mean squared temperature error divided by the mean squared temperature excursions between the neighboring observations at each level. The details about the estimation scheme can be found in Appendix A. Once the neighboring observed temperature profiles are provided, the diffusion coefficient can be estimated using the scheme.

[14] The water temperature observed at Station A from 1954 to 1985 was not uniformly sampled. The original data were reprocessed to generate a climatological vertical temperature data set with about 10-day resolution, namely, three profiles per month. A year is divided into 36 spans, with three spans for each month. The first and second spans of each month contain ten days, while the third span contains the remaining days. All the observed data are then classified into the 36 spans. Quality control is applied to the temperature observations in every span to remove the bugs. The remaining data are averaged to form 36 temperature pro-

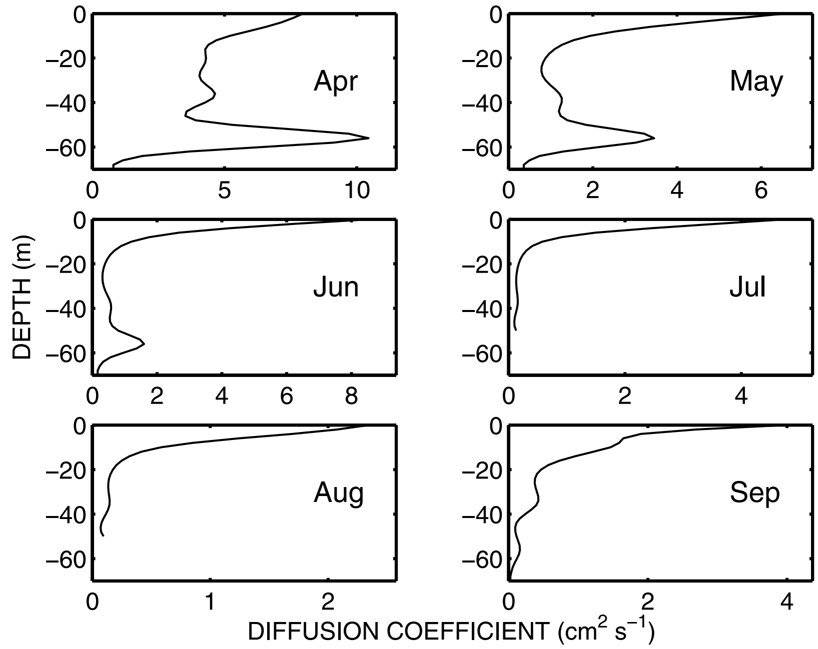

Figure 6. Monthly estimated diffusion coefficient at Station A.

files. The annual cycle of temperature at several selected levels derived from this data set is shown in Figure 2.

[15] The original temperature observations were taken at 0 m, 5 m, 10 m, 15 m, 20 m, 25 m, 30 m, 35 m, 50 m, and 70 m levels. Therefore, the diffusion coefficients can be estimated only from 0 m to 70 m (9 m above the bottom). In order to facilitate the numerical calculation, we interpolated the standard level data set linearly onto 1.0 m intervals. The bottom boundary condition requires that the bottom temperature must be the same as the one at the nearest higher level. So an additional pseudo level of 71 m with the same temperature as 70 m was added to the profile. Note that the temperature variation is not controlled by diffusion when convection occurs. Thus, it is difficult to obtain a reasonable diffusion coefficient in autumn and winter using the above diffusion equation. In this study, only the temperature data from April to September are used to estimate the diffusion coefficient. Since the temperature observations were reprocessed into the data set with 10-day resolution, three profiles of diffusion coefficients can be obtained for every month from the estimation scheme. A total of 18 profiles are finally obtained. Figure 6 shows monthly profiles of the diffusion coefficient.

[16] One can see that the diffusion coefficient profiles share a common feature. The diffusion coefficient has a maximum at the surface, and then gradually decreases down to about 20 m level. In the middle layer (20–40 m), the coefficients are smaller than those in the surface layer. A peak value is found near 55 m from April to June. The vertical resolution of the original temperature observations is not high enough to describe the behavior in bottom mixed layer (about 50–70 m at Station A). Thus, it should be noted that the estimated diffusion coefficients below 50 m might not give the detailed information about the bottom mixing. Therefore, high vertical resolution observations are necessary to further solve this issue. On the other hand, equation (4) with boundary conditions (5) and (6) requires that the bottom temperature increase monotonously from March to December because of the assumption that the surface heat flux could only be conveyed downward by diffusion. This is opposite to the observed bottom temperature which actually decreases with time in July and August as shown in Figure 2. A previous study had revealed that the YSCWM shifts its location with time [*Su and Yuan*, 2005]. Thus, the diffusion coefficients from 50 m to 70 m in July and August may include large errors, and they are not included in Figure 6.

[17] Figure 6 shows the seasonal variability of diffusion coefficient. In April, the surface is heated by the increasing heat flux while the thermocline is still weak, which results in a large diffusion coefficient in the surface and middle layer. As the surface temperature becomes warmer and the thermocline becomes stronger, the heat flux becomes more difficult to convey to the subsurface layer. So the diffusion coefficient in the middle layer is smaller in the summer months of June, July, and August.

[18] The mean diffusion coefficient (MDC) in the upper layer (0–15 m) and middle layer (20–40 m) are listed in Table 1. One can see that the MDC in the upper layer is 3.5 to 12 times as large as that in the middle layer from May to September. In April, the MDCs in the upper and middle layers are larger than those from May to September. Averaged from June to September, the mean MDC in the middle layer is 0.28 cm^2 s^{-1}, a value close to the background mixing coefficient of 0.20 cm^2 s^{-1} as specified in the POM model.

Table 1. Mean Diffusion Coefficient Estimated From Temperature Observations at Station A

	Apr	May	Jun	Jul	Aug	Sep
Upper layer, cm^2 s^{-1}	6.2	3.4	3.3	1.8	1.2	1.9
Middle layer, cm^2 s^{-1}	4.3	0.98	0.42	0.15	0.14	0.39

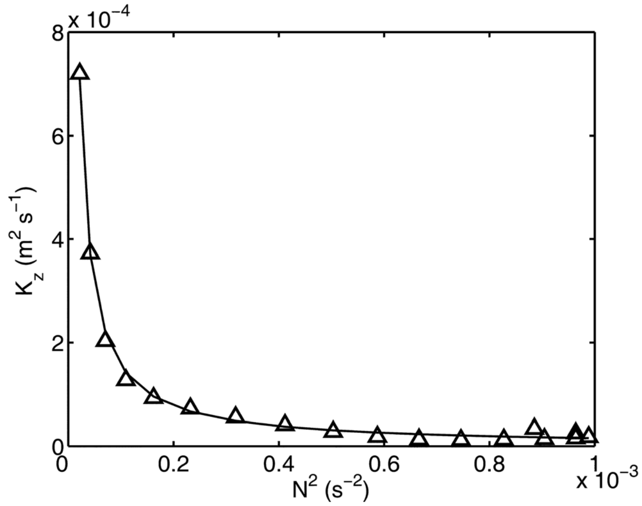

Figure 7. Estimated diffusion coefficient (k_z) versus the squared buoyancy frequency (N^2) in the middle layer at Station A. Triangles present the data from April to September. The solid line presents $k_z = 1.55 \times 10^{-8} m^2 s^{-3}/N^2$.

[19] As analyzed above, the diffusion coefficient is a key parameter to explain the temperature variation in the central YS. In general, the strength of diapycnal mixing is related to oceanic stratification and turbulence energy dissipation. *Osborn* [1980] derived a formula to calculate the diapycnal diffusivity k_ρ,

$$k_\rho = \gamma \frac{\varepsilon}{N^2}, \tag{7}$$

where N is the buoyancy frequency, ε the turbulence energy dissipation rate, and γ the mixing efficiency. When the turbulence energy dissipation rate is fixed, the diapycnal diffusivity is inversely proportional to the squared buoyancy frequency. We find that the inverse proportion is applicable to the estimated diffusion coefficient from April to September at Station A, as shown in Figure 7. For every profile of the estimated diffusion coefficients, we average the values in the middle layer and obtain a mean diffusion coefficient. In the same way, a mean value of the squared buoyancy frequencies in the middle layer is also calculated from the observed temperature and salinity. A total of eighteen mean diffusion coefficients and eighteen mean squared buoyancy frequencies are finally obtained. Their relation is illustrated in Figure 7. It is obvious that the diffusion coefficient is inversely proportional to the squared buoyancy frequency. The proportionality coefficient is about $1.55 \times 10^{-8} m^2 s^{-3}$, i.e.,

$$k_z = \frac{1.55 \times 10^{-8} m^2 s^{-3}}{N^2}. \tag{8}$$

Comparing equation (7) with equation (8), one can see that the proportionality coefficient actually represents the efficiency times the turbulence energy dissipation rate. Thus, a constant proportionality coefficient implies that the averaged turbulence energy dissipation rate from 1954 to 1985 was invariant with seasons at Station A, if the mixing efficiency is considered to be constant. However, this inference is difficult to be validated in this study due to the lack of actual observations of turbulence energy dissipation rate.

4. Discussion

[20] The MASNUM coupled model is used to simulate the circulation and the thermal structure in the YS in this study. It would be of interest to compare the estimated diffusion coefficient with the diffusion coefficient actually used in the wave-tide-circulation model. The estimated diffusion coefficients below 50 m could not give reliable information because the vertical resolution of the original temperature observations is not high enough to describe the bottom mixed layer (about 50–70 m at Station A). Only the diffusion coefficients from 0 m to 50 m in the coupled model are shown in Figure 8, which illustrates the monthly diffusion coefficient from April to September at Station A. One can see a similar case to Figure 6, i.e., the diffusion coefficient in the coupled model is large at the surface, and then decreases gradually downward from April to August. The minimum diffusion coefficient, 0.20 $cm^2 s^{-1}$, which is the background mixing specified in the POM model, occurs in the middle layer. This means that both the wave-induced and the tide-induced mixings cannot reach the middle layer where the background mixing dominates. For the levels below 40 m, the diffusion coefficient increases downward from April to August. The increasing diffusion coefficient could be attributed to the effect of tide-induced mixing.

[21] There are several differences between the estimated diffusion coefficient and that used in the model. First, Figure 8 shows that the simulated depth of upper mixed layer is about 10 m from April to August, while the profiles of estimated diffusion coefficients reveal that the depth is about 15 m. This suggests that the wave-induced mixing used in the coupled model is still not enough to present the real upper mixed layer although the modeled upper mixed layer is much more reasonable than the result generated by the original POM model [*Qiao et al.*, 2004a, 2004b]. Second, one can see from Figure 8 that the diffusion coefficient is almost a constant in the middle layer, i.e., k_z = 0.20 cm^2 s^{-1}. However, the estimated diffusion coefficient reveals a seasonal variation in the same layer, as shown in Figure 6 and Table 1. Even so, the mean value of the estimated diffusion coefficients in the middle layer averaged from June to September, 0.28 cm^2 s^{-1}, is close to the background mixing coefficient of 0.20 cm^2 s^{-1} in the POM model.

[22] In order to check the dependence of the estimated diffusion coefficient on the number of the temperature observations being used, the total original temperature observations at Station A are divided into two groups. Group 1 contains the data observed before 1970 (including 1970), which includes about 25% of the total original data. The remaining data set forms Group 2. Repeating the procedures in section 3, the respective diffusion coefficients from the two groups of data are estimated as shown in Figure 9. One can see that the profiles of the estimated diffusion coefficients are similar in June, August, and September, but some differences are noted for those in April, May, and July. In the upper and middle layers, the

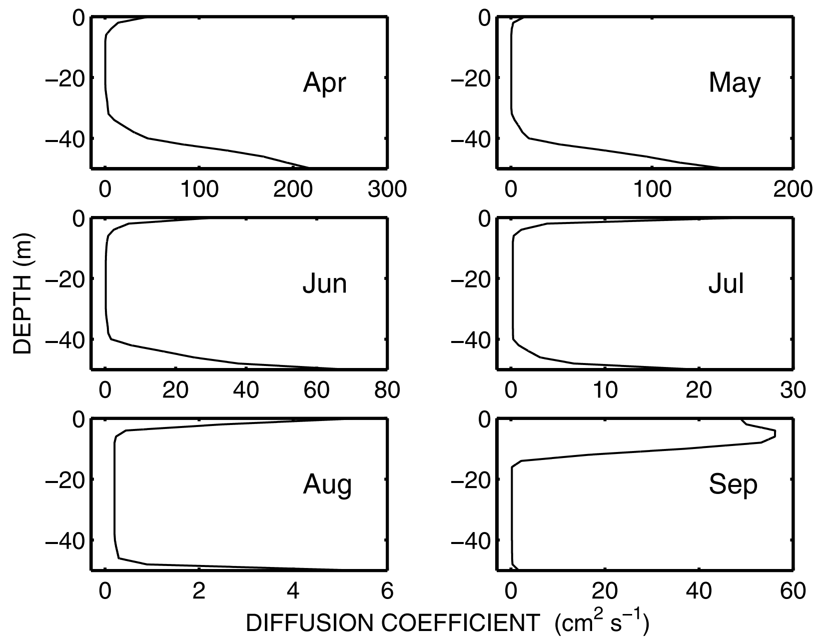

Figure 8. Monthly diffusion coefficient in the coupled model at Station A.

MDCs of Group 1 are consistent with those in Group 2 in June, August, and September (Table 2). In May, the diffusion coefficients of Group 1 are smaller than those of Group 2 at the levels above 30 m, while the reverse is true for those below 40 m. In July, the diffusion coefficients of Group 1 are smaller than those of Group 2 in all layers. Despite those differences in individual values, the vertical structures of the diffusion coefficients of the two groups are similar in the two months. In April, the coefficient profile of Group 1 is clearly different from that of Group 2. This could be due to a weak stratification in April and a small number of data being used in Group 1. In fact, the study area does not form a strong thermocline in April. Any synoptic atmospheric process may influence the temperature from the surface to the bottom, thus contributing to the estimated diffusion coefficients. When the number of observations is statistically insufficient, the effects of synoptic atmospheric processes cannot be properly removed from the monthly climatological mean. Thus, enough observations are necessary to obtain a mean status of the temperature structure. In Figure 6, the diffusion coefficients are estimated from enough temperature observations with the number of orig-

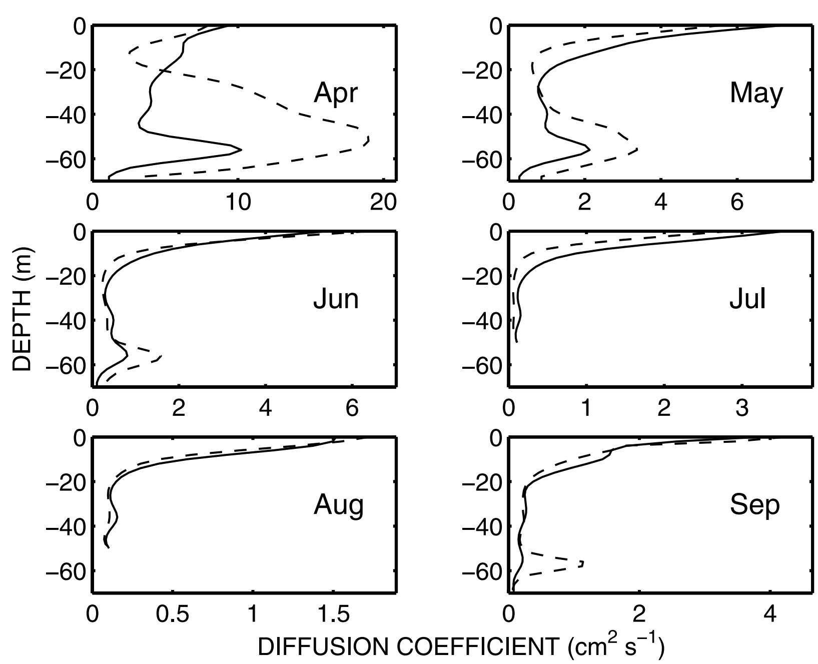

Figure 9. Diffusion coefficient estimated from the temperature observations at Station A. Dashed line: Group 1 (before 1970); solid line: Group 2 (after 1970).

Table 2. Mean Diffusion Coefficient Estimated From Temperature Observations at Station A Before (Group 1) and After 1970 (Group 2)

		Apr	May	Jun	Jul	Aug	Sep
Upper layer, $cm^2\ s^{-1}$	Group 1	4.9	2.5	2.5	1.0	0.88	1.8
	Group 2	7.0	4.0	2.6	1.7	1.0	1.9
Middle layer, $cm^2\ s^{-1}$	Group 1	10.3	0.89	0.28	0.06	0.10	0.23
	Group 2	4.1	0.9	0.38	0.15	0.13	0.27

inal temperature profiles of about 95 per month. Therefore, the diffusion coefficients in Figure 6 represent the realistic means from 1954 to 1985.

[23] Figure 10 shows the estimated diffusion coefficients versus the squared buoyancy frequency in the middle layer before and after 1970. The inverse relationship between the diffusion coefficients and the squared buoyancy frequency is represented in the two groups of data. The proportionality coefficient remains at about $1.55 \times 10^{-8}\ m^2\ s^{-3}$. The different temperature observations between the two groups of data do not influence the proportionality relationship.

[24] As pointed out earlier, the proportionality coefficient being a constant as illustrated in Figures 7 and 10 implies that the turbulence energy dissipation rate in the middle layer averaged from 1954 to 1985 is invariant with season at Station A. Generally, the winds and tides are the only two possible sources of mechanical energy to drive the interior mixing [*Munk and Wunsch*, 1998]. Semidiurnal tides are dominant in the YS and the tides show little variation with season [*Fang et al.*, 2004]. It therefore seems reasonable to consider the tides as a stationary energy source for the diapycnal mixing. Monthly climatological wind speeds at Station A from COADS [*da Silva et al.*, 1994a, 1994b] are shown in Figure 11. The wind speeds show an equable behavior from April to September although they are obviously larger in winter than those in summer. During the time period from April to September, the maximum wind speed is 6.3 ms^{-1} (in April) and the minimum is 5.4 ms^{-1} (in June), with a standard deviation of 0.32 ms^{-1}. The small variation in wind speeds implies that the energy from the winds to derive the diapycnal mixing could almost be invariant at Station A from April to September. It is therefore not surprising that a constant proportionality coefficient exists between the diffusion coefficient and the squared buoyancy frequency, as illustrated in Figures 7 and 10.

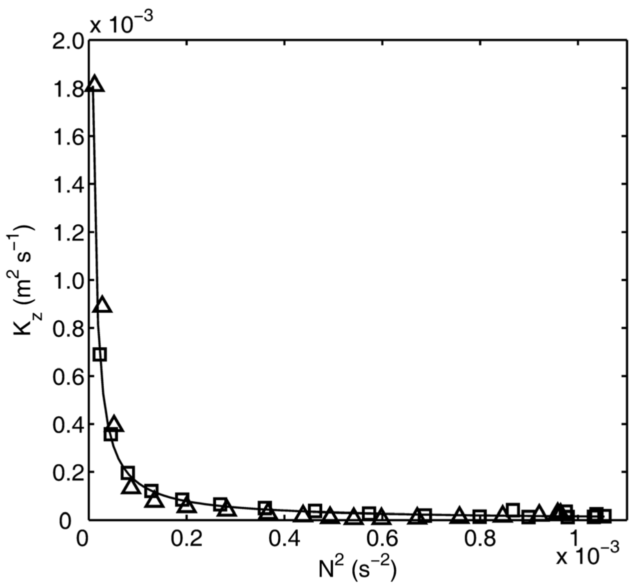

Figure 10. Estimated diffusion coefficient (k_z) versus the square of buoyancy frequency (N^2) in the middle layer at Station A. Triangles represent the data of Group 1 (before 1970) from April to September. Squares represent the data of Group 2 (after 1970). The solid line represents $k_z = 1.55 \times 10^{-8} m^2 s^{-3}/N^2$.

[25] It should be noted that the temperature diffusion equation is the one being used to establish the scheme for the estimation of the diffusion coefficient. Neglecting the advection terms induces an uncertainty in the estimated diffusion coefficient. In this study, this uncertainty is estimated by using the results from the MASNUM coupled model. The results show that the ratio of the diffusion term to the advection terms is larger than 5 from the surface to the bottom in the central YS. This indicates that the estimated diffusion coefficients, as shown in Figures 6 and 9, represent reality at Station A. However, it should be kept in mind that the scheme, used in this study to estimate the diffusion coefficient, is applicable only when diffusion controls the temperature variation.

5. Summary

[26] This study provides an insight into the mechanisms of seasonal temperature variation in the YS. The temperature observations from 1954 to 1985 show that the bottom temperature lags 3–4 months behind the surface temperature in reaching a maximum in the central YS. The MASNUM wave-tide-circulation coupled model is used to simulate the seasonal variation of temperature and to investigate the dominant physical process which controls the temperature variation below the surface layer. The coupled model reproduces the observed time lag phenomena. Further analysis

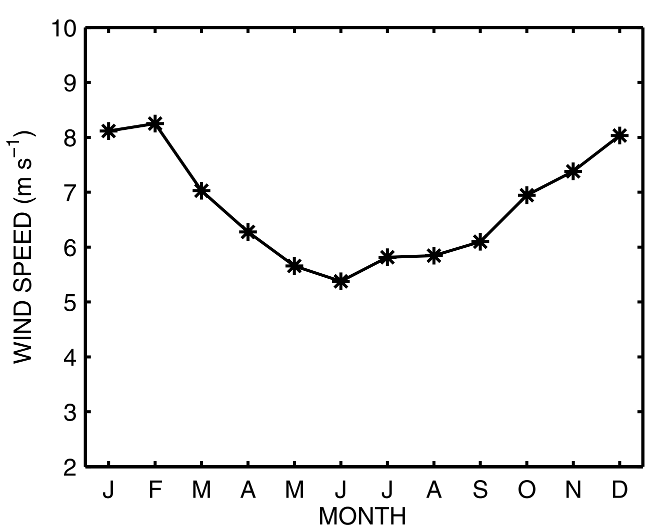

Figure 11. Monthly climatological wind speeds at Station A.

indicates that the diffusion process is the key factor governing the temperature variation below the surface layer.

[27] Based on the diffusion equation of temperature, a scheme has been developed to estimate the diffusion coefficient from temperature observations by inverse methods. The cost function is specified as the mean squared temperature error divided by the mean squared temperature excursion between two continuous observation profiles. At Station A (36°00′N, 124°00′E), the diffusion coefficient is estimated for the time period from April to September. The diffusion coefficient profiles share a common feature. The coefficient peaks at the surface, and then decreases with depth down to 20 m. In the middle layer (from 20 to 40 m), the coefficient remains small. The MDCs are almost one order of magnitude smaller in the middle layer than the upper layer (from 0 to 15 m), except in April. The mean MDC in the middle layer, averaged from June to September, is 0.28 $cm^2\ s^{-1}$. In addition, the estimated diffusion coefficient in the middle layer is found to be inversely proportional to the squared buoyancy frequency with the proportionality coefficient of about $1.55 \times 10^{-8} m^2\ s^{-3}$. The inverse proportionality is consistent with the Osborn's relation if the turbulence energy dissipation rate is assumed to be a constant.

Appendix A: A Scheme to Estimate the Diffusion Coefficient

[28] Numerical results indicate that the diffusion is dominant for the water temperature variation below the surface layer in the central YS, i.e.,

$$\frac{\partial T}{\partial t} = \frac{\partial}{\partial z}\left(k_z \frac{\partial T}{\partial z}\right). \tag{A1}$$

To close the equation, boundary conditions are needed. For simplicity, the surface temperature rather than the surface heat flux is specified as the surface boundary condition,

$$T|_{z=0} = T_{surf}(t). \tag{A2}$$

T_{surf} can be provided by observed surface temperature variation for estimating the diffusion coefficient. The bottom boundary condition is specified as zero flux. In general, the topographic slope is gentle. Therefore, the bottom boundary condition can be written as

$$\frac{\partial T}{\partial z}|_{z=-H} = 0. \tag{A3}$$

Discretizing equation (A1) yields

$$T_i^m = T_i^{m-1} + \frac{(k_z)_i \delta t}{(\delta z)^2}\left(T_{i+1}^{m-1} - T_i^{m-1}\right) - \frac{(k_z)_{i-1}\delta t}{(\delta z)^2}\left(T_i^{m-1} - T_{i-1}^{m-1}\right), \tag{A4}$$

where the superscripts denote the time step index and the subscripts the vertical grid index. δt and δz are the time step and vertical grid spacing, respectively. When the initial temperature profile, the surface temperature variation, and the diffusion coefficient are all provided, the temperature variations at other levels can be calculated by using equation (A4) with the boundary conditions (A2) and (A3). In general, it is difficult to obtain the diffusion coefficient in the real ocean. We apply a method to invert for the diffusion coefficient from the continuous temperature profiles.

[29] Let $\tilde{T}_i^1$ and $\tilde{T}_i^2$ denote the continuous temperature profiles observed at time t_1 and t_2, the time interval $t_2 - t_1 = M\ \delta\ t$. Surface temperature used in the upper boundary condition can be obtained by linearly interpolating from $\tilde{T}_i^1$ and $\tilde{T}_i^2$. Once an initial guess profile for the diffusion coefficient is provided, k_{si} , the temperature profile can be calculated using equation (A4). After M time steps, we obtain T_i^M.

[30] The cost function for inverting for the diffusion coefficient k_z is defined as

$$F = \sum_{i=1}^{I}\left(\frac{T_i^M + \delta T_i^M - \tilde{T}_i^2}{R_i}\right)^2, \tag{A5}$$

where R_i is a weighting coefficient which is specified as the temperature excursions between the two continuous temperature profiles, i.e., $R_i = |\tilde{T}_i^2 - \tilde{T}_i^1|$, δT_i^M denotes the change in temperature due to $\delta\ k_s$, then we have

$$\delta T_i^M = \sum_{l=1}^{I}\frac{\partial T_i^M}{\partial (k_s)_l}(\delta k_s)_l. \tag{A6}$$

The cost function F can reach the local minimum value as long as

$$\frac{\partial F}{\partial (k_s)_j} = 0, \tag{A7}$$

that is

$$\sum_{i=1}^{I}\frac{2}{R_i^2}\left(T_i^M - \tilde{T}_i^2 + \sum_{l=1}^{I}\frac{\partial T_i^M}{\partial (k_s)_l}(\delta k_s)_l\right)\frac{\partial T_i^M}{\partial (k_s)_j} = 0. \tag{A8}$$

Equation (A8) with j from 1 to I is a group of equations with the variables $(\delta k_s)_j$, $j = 1, 2, \ldots I$. We obtain δk_s by solving the group of equations. $\frac{\partial T_i^M}{\partial (k_s)_j}$ can be calculated from equation (A4). Defining

$$D_{i,j}^m = \frac{\partial T_i^m}{\partial (k_z)_j}, \tag{A9}$$

we obtain the iterative equation

$$D_{i,j}^{m+1} = D_{i,j}^m + \frac{\delta_{i,j}\delta t}{(\delta z)^2}\left(T_{i+1}^m - T_i^m\right) - \frac{\delta_{i-1,j}\delta t}{(\delta z)^2}\left(T_i^m - T_{i-1}^m\right) + \frac{(k_z)_i\delta t}{(\delta z)^2} \cdot \left(D_{i+1,j}^m - D_{i,j}^m\right) - \frac{(k_z)_{i-1}\delta t}{(\delta z)^2}\left(D_{i,j}^m - D_{i-1,j}^m\right), \tag{A10}$$

where $\delta_{i,j}$ is the Kronecker operator,

$$\delta_{i,j} = \begin{cases} 0, & \text{for} \quad i \neq j, \\ 1, & \text{for} \quad i = j. \end{cases} \tag{A11}$$

From equation (A10), one can get $\frac{\partial T_i^M}{\partial (k_s)_j}$.

[31] After getting $(\delta k_s)_i$, a new guess value for the diffusion coefficient, k'_s, can be calculated,

$$k'_{si} = k_{si} + \delta k_{si}. \tag{A12}$$

After repeating the above processes, one can get the profile of diffusion coefficient. Tests show that the inversion scheme is convergent. $F = 0.01$ is specified as a criterion to judge whether the estimation process can be terminated or not. If the cost function F is larger than 0.01, the estimation process continues. If F is less than 0.01, the estimation process is terminated and the profile of diffusion coefficient is accepted. It is worth noting that the estimated diffusion coefficient from the neighboring temperature profiles observed at times t_1 and t_2 is invariant during the time period between t_1 and t_2. The variation of diffusion coefficient with time can be obtained by estimating the diffusion coefficient from a series of temperature profiles observed at times $t_1, t_2, \ldots t_N$.

[32] **Acknowledgments.** We were truly thankful to S. C. Lee at FIO, X. Huang at FIO, Q. Zheng at Maryland University, and the anonymous reviewers for smoothing the language. Comments given by the two anonymous reviewers greatly improved this manuscript. This study was supported by the China National Key Basic Research Program through grant G1999043809 and the National Natural Science Foundation of China through grants 40476017 and 40406008.

References

Chu, P. C., C. R. Fralick, S. D. Haeger, and M. J. Carron (1997), A parametric model for Yellow Sea thermal variability, *J. Geophys. Res.*, *102*, 10,499–10,508.

Chu, P. C., Y. Chen, and A. Kuninaka (2005), Seasonal variability of the Yellow Sea/East China Sea surface fluxes and thermohaline structure, *Adv. Atmos. Sci.*, *22*, 1–20.

da Silva, A. M., C. C. Young, and S. Levitus (1994a), *Atlas of Surface Marine Data 1994,* vol. 3, *Anomalies of Heat and Momentum Fluxes, NOAA Atlas NESDIS 8,* 411 pp., U.S. Dep. of Commer., Natl. Oceanic and Atmos. Admin., Silver Spring, Md.

da Silva, A. M., C. C. Young, and S. Levitus (1994b), *Atlas of Surface Marine Data 1994,* vol. 4, *Anomalies of Fresh Water Fluxes, NOAA Atlas NESDIS 9,* 308 pp., U.S. Dep. of Commer., Natl. Oceanic and Atmos. Admin., Silver Spring, Md.

Ezer, T. (2000), On the seasonal mixed layer simulated by a basin-scale ocean model and the Mellor-Yamada turbulence scheme, *J. Geophys. Res.*, *105*, 16,843–16,855.

Fang, G., Y. Wang, Z. Wei, B. H. Choi, X. Wang, and J. Wang (2004), Empirical cotidal charts of the Bohai, Yellow, and East China Seas from 10 years of TOPEX/Poseidon altimetry, *J. Geophys. Res.*, *109*, C11006, doi:10.1029/2004JC002484.

Feng, M., D. Hu, and Y. Li (1992), A theoretical solution for the thermohaline circulation in the Southern Yellow Sea, *Chin. J. Oceanol. Limnol.*, *10*, 289–300.

He, C., Y. Wang, and Z. Lei (1959), A preliminary study on the generation and the characteristics of the Cold Water Mass of the Yellow Sea (in Chinese with English abstract), *Oceanol. Limnol. Sin.*, *2*, 11–15.

Jin, M., Z. Wang, and B. Xu (1996), Three-dimensional numerical prediction of vertical structure of the Huanghai and Bohai Seas (in Chinese with English abstract), *J. Oceanogr. Huanghai Bohai Seas*, *14*, 67–74.

Kantha, L. H., and C. A. Clayson (1994), An improved mixed layer model for geophysical applications, *J. Geophys. Res.*, *99*, 25,235–25,266.

Kwan, P. (1963), A preliminary study of the temperature variation and the characteristics of the circulation of the Cold Water Mass of the Yellow Sea (in Chinese with English abstract), *Oceanol. Limnol. Sin.*, *5*, 255–284.

Levitus, S. (1982), Climatological atlas of the world ocean, *NOAA Prof. Pap. 13,* 173 pp. plus 17 microfiche, U.S. Govt. Print. Off., Washington, D. C.

Martin, P. J. (1985), Simulation of the mixed layer at OWS November and Papa with several models, *J. Geophys. Res.*, *90*, 581–597.

Mellor, G. L. (2001), One-dimensional, ocean surface layer modeling, a problem and a solution, *J. Phys. Oceanogr.*, *31*, 790–809.

Mellor, G. L., and T. Yamada (1982), Development of a turbulence closure model for geophysical fluid problems, *Rev. Geophys.*, *20*, 851–875.

Miao, J., X. Liu, and Y. Xue (1991), A preliminary study on the generation mechanism of the Cold Water Mass in the North Yellow Sea (in Chinese), 1. Model, *Sci. China, Ser. B*, *20*, 131–132.

Munk, W., and C. Wunsch (1998), Abyssal recipes II: energetics of tidal and wind mixing, *Deep Sea Res.*, *45*, 1977–2010.

Osborn, T. (1980), Estimates of the local rate of vertical diffusion from dissipation measurements, *J. Phys. Oceanogr.*, *10*, 83–89.

Qiao, F., J. Ma, Y. Yang, and Y. Yuan (2004a), Simulation of the temperature and salinity along 36°N in the Yellow Sea with a wave-current coupled model, *J. Korea Soc. Oceanogr.*, *39*, 35–45.

Qiao, F., Y. Yuan, Y. Yang, Q. Zheng, C. Xia, and J. Ma (2004b), Wave-induced mixing in the upper ocean: Distribution and application to a global ocean circulation model, *Geophys. Res. Lett.*, *31*, L11303, doi:10.1029/2004GL019824.

Su, J., and D. Huang (1995), On the current field associated with the Yellow Sea cold water mass (in Chinese with English abstract), *Oceanol. Limnol. Sin.*, *26*, 1–7.

Su, J., and Y. Yuan (2005), *Hydrology in the China Seas* (in Chinese), pp. 1–367, Ocean Press, Beijing.

Wang, Z., B. Xu, E. Zou, K. Yang, and F. Li (1996a), A study on the numerical prediction method for the vertical thermal structure in the Bohai and Huanghai Seas. 1. One-dimensional numerical prediction model (in Chinese with English abstract), *J. Oceanogr. Huanghai Bohai Seas*, *14*, 37–45.

Wang, Z., F. Li, B. Gong, B. Xu, and E. Zou (1996b), A study on the numerical prediction method for the vertical thermal structure in the Bohai and Huanghai Seas. 2. A quasi-three-dimensional numerical prediction model (in Chinese with English abstract), *J. Oceanogr. Huanghai Bohai Seas*, *14*, 46–57.

Xia, C., F. Qiao, M. Zhang, Y. Yang, and Y. Yuan (2004a), Simulation of double cold cores of the 35°N section in the Yellow Sea with a wave-tide-circulation coupled model, *Chin. J. Oceanol. Limnol.*, *22*, 292–298.

Xia, C., F. Qiao, Q. Zhang, and Y. Yuan (2004b), Numerical modeling of the quasi-global ocean circulation based on POM, *J. Hydrodyn., Ser. B*, *16*, 537–543.

Xia, C., F. Qiao, Y. Yang, J. Ma, and Y. Yuan (2006), Three-dimensional structure of the summertime circulation in the Yellow Sea from a wave-tide-circulation coupled model, *J. Geophys. Res.*, *111*, C11S03, doi:10.1029/2005JC003218.

Yuan, Y. (1979), Circulation of the Cold Water Mass of the Yellow Sea, 1. thermal structure and the characteristics of circulation in the correlation coefficient of Cold Water Mass (in Chinese with English abstract), *Oceanol. Limnol. Sin.*, *10*, 187–199.

Yuan, Y., and H. Li (1993), The study of circulation structure and producing mechanism of Yellow Sea Cold Water Mass (in Chinese), *Sci. China, Ser. B*, *23*, 93–103.

Yuan, Y., Z. Pan, F. Hua, and L. Sun (1991), LAGDF-WAM numerical wave model, *Acta Oceanol. Sin.*, *10*, 483–488.

D. Dai, F. Qiao, and C. Xia, The First Institute of Oceanography, State Oceanic Administration (SOA), 6 Xianxialing Road, Hi-tech Industry Park, Qingdao 266061, China. (qiaofl@fio.org.cn)

K. T. Jung, Korea Ocean Research and Development Institute, Ansan 425-600, Korea.